

**Metric for quantifying elastic and inelastic thermal transport at interfaces**Yixin Xu  and Yanguang Zhou <sup>\*</sup>*Department of Mechanical and Aerospace Engineering, The Hong Kong University of Science and Technology, Clear Water Bay, Kowloon, Hong Kong SAR* (Received 21 May 2024; revised 14 August 2024; accepted 26 August 2024; published 12 September 2024)

Understanding interfacial thermal transport across interfaces is crucial for unraveling heat transfer mechanisms in materials and devices. Interestingly, an effective metric to quantify the contributions from elastic and inelastic vibration scatterings at interfaces to interfacial thermal transport is still lacking. In this paper, we demonstrate that the significance of elastic and inelastic vibration scatterings at the interfaces on the interfacial thermal transport is determined by the competition between the similarity of vibrational density of states (VDOS) between two contacted leads and the anharmonicity of the interface. The VDOS similarity between two contacted leads, measured using the Kullback-Leibler (K-L) divergence value, is found to correlate strongly to the signature of elastic thermal transport at interfaces. Our calculations show that elastic vibration scatterings dominate the interfacial thermal transport at interfaces when its K-L divergence value is  $<0.2$ . For instance, the elastic vibration scatterings contribute  $>75\%$  to the interfacial thermal conductance (ITC) of Ar/heavy Ar (h-Ar) interfaces when the K-L divergence value is  $<0.2$ . When the K-L divergence value is  $>0.2$ , which indicates the VDOS similarity between two contacted leads is significant, we find that both the elastic and inelastic vibration scatterings at interfaces contribute primarily to the interfacial thermal transport. Furthermore, for the interfaces with K-L divergence values  $>1$ , the ratio of ITC contributed by inelastic vibration scatterings can be quantitatively characterized by the interfacial anharmonic ratio (IAR), which is a measure of interfacial anharmonicity. Our calculations on Ar/h-Ar, Si/Al, and Si/Ge interfaces at various temperatures with K-L divergence values  $>1$  show that the IAR is generally linear with the inelastic contribution to ITC with an error of 12.5%. Our results here advance the fundamental understanding of interfacial thermal transport resulting from elastic or inelastic vibration scatterings, which may benefit the thermal management design in related applications.

DOI: [10.1103/PhysRevB.110.115305](https://doi.org/10.1103/PhysRevB.110.115305)**I. INTRODUCTION**

Interfaces in heterogeneous materials offer many possibilities for designing the corresponding devices with engineered electrical and thermal properties. The thermal transport across interfaces, particularly in heterojunctions of electronics and thermoelectrics, is crucial for designing and optimizing their performance.

Vibration scatterings at interfaces have been widely studied, mainly through the acoustic mismatch model (AMM) [1], the diffuse mismatch model (DMM) [2], and the harmonic nonequilibrium Green's function (NEGF) [3–6], and permutations thereof that only include contributions from elastic vibration process while neglecting inelastic processes. The interfacial thermal conductance (ITC) of some systems, such as Al/Si [7], Al/GaN [8], and TiN/Al<sub>2</sub>O<sub>3</sub> [9], predicted using these methods agrees well with experimental measurements, which indicates the elastic vibration scatterings are the main heat transfer channels at these interfaces. However, some experiments have implied that the inelastic vibration scatterings at diamond/Pt and diamond/Au interfaces contribute largely to the ITC by comparing the upper limit of elastic ITC with

the measured value [10]. Many methods based on NEGF [11–13], equilibrium molecular dynamics (EMD) [14–16], or non-EMD (NEMD) [17–20] are then developed to quantify the contribution of inelastic vibration scatterings to ITC. For instance, Dai and Tian [11] extended the NEGF to include three-vibration scatterings at interfaces and found that the three-vibration scattering process contributes  $\sim 27\%$  to the ITC of Si/Ge at room temperature. For another example, Zhou and Hu [18] characterized the three-vibration scatterings at the interface in the framework of NEMD and showed that three-vibration scatterings result in  $\sim 20\text{--}30\%$  of the ITC of the Si/Ge interfaces. Based on EMD or NEMD simulations, all high-order inelastic vibration scatterings are found to contribute even higher to the ITC of interfaces, e.g.,  $\sim 50\%$  for Si/Ge interfaces at room temperature in the framework of NEMD [21],  $\sim 50\%$  for Si/Al interfaces at 700 K in the framework of NEMD [22], and  $\sim 50\%$  for Si/Ge interfaces in the framework of EMD [16]. While there is great progress in quantifying the vibration transport across interfaces, the underlying mechanism behind the interfacial thermal transport is still poorly understood (e.g., the factors governing the elastic and inelastic processes at interfaces remain unclear), and a metric for quickly characterizing the contribution to ITC from elastic and inelastic vibration scattering processes is lacking. At the same time, a quick metric to determine the

<sup>\*</sup>Contact author: maeygzhou@ust.hk

contributions to interfacial thermal transport from elastic and inelastic scatterings directly guides us in designing interfacial thermal materials for thermal regulation. On the one hand, we may increase the interfacial thermal transport by improving elastic scatterings at the interface [23–25]. On the other hand, inelastic scatterings usually become significant at elevated temperatures, which can further enhance interfacial thermal transport at high temperatures [8,18,22]. By comprehending these two metrics, we can quickly construct interfacial structures with multilayers to optimize interfacial thermal transport across a wide temperature range.

In this paper, we find that the contribution to the ITC from elastic and inelastic vibration scatterings is determined by the competition between the similarity of the vibrational density of states (VDOS) between two contacted leads and the interfacial anharmonicity. The Kullback-Leibler (K-L) divergence value and interfacial anharmonic ratio (IAR) are further proposed to measure the VDOS similarity and the interfacial anharmonicity, respectively. Our results show that, even at high temperatures (e.g.,  $T = 40$  K for the Ar/h-Ar interface), the elastic vibration contribution to ITC is  $>80\%$  for these interfaces with a small K-L divergence value  $<0.2$ . When the K-L divergence value of interfaces is  $>0.2$ , both elastic and inelastic vibration scatterings contribute largely to ITC. The contributions to ITC from elastic and inelastic vibration scatterings can be further quantitatively characterized by the IAR when the K-L divergence value is  $>1.0$ . Our calculations on Ar/h-Ar, Si/Al, and Si/Ge interfaces at various temperatures with K-L divergence values  $>1.0$  show that the IAR is linear with the inelastic vibration contribution to ITC with an error bar of 12.5%. The paper is organized as follows. In Sec. II A, we introduce the method based on NEMD simulations to quantify the contributions to ITC from elastic and inelastic vibration scatterings. The calculation details and physical explanations of the K-L divergence value and IAR are given in Sec. II B. Results and discussions are presented in Sec. III. The influence of VDOS similarity and interfacial strength on the interfacial thermal transport is discussed in Secs. III A and III B, respectively. The interfacial anharmonicity on the interfacial thermal transport is further discussed in Sec. III C. In the following Sec. IV, we propose the generalized descriptor for quantifying the contributions to ITC from elastic and inelastic vibration scatterings in various systems. Conclusions are drawn in Sec. V.

## II. METHOD AND SIMULATION DETAILS

### A. Quantifying the interfacial thermal transport based on NEMD simulations

To quantify the interfacial thermal transport in the framework of NEMD simulations (Appendix A), we calculate the heat current across the interface using [18,19,26,27]

$$Q_{L \rightarrow R} = \frac{1}{4} \sum_i^L \sum_j^R \left\langle \left( \frac{\partial U_{ji}}{\partial \vec{r}_{ji}} - \frac{\partial U_{ij}}{\partial \vec{r}_{ij}} \right) \cdot (\vec{v}_i + \vec{v}_j) \right\rangle, \quad (1)$$

in which  $\langle \rangle$  denotes the time average in NEMD simulations, and  $\vec{v}_i$ ,  $\vec{r}_{ij}$ , and  $U_{ij}$  are atomic velocity, relative displacement, and potential energy of the atom pair  $i$  and  $j$ , respectively. For

the two-body potential, the atomic potential partial function can be written as the atomic forces, e.g.,  $\vec{F}_{ij} = \partial U_{ij} / \partial \vec{r}_{ij}$ . Here, we output atomic velocity  $\vec{v}_i$  and the atomic potential partial function  $\partial U_{ij} / \partial \vec{r}_{ij}$  every 20 fs after NEMD simulations reach the steady state. Here,  $L$  and  $R$  represent the left and right sides along the ideal interface with no thickness and constitute the interfacial region. The size of the interfacial region is set as one unit cell length at both sides of the interface, which is large enough to obtain the convergent heat current [19,26]. It is also noted that the interfacial heat current calculated using Eq. (1) is identical to the heat current calculated via  $Q = \langle dE/dt \rangle$  in NEMD simulations [26].

By introducing the cross-correlation function between velocity and the atomic partial potential function, the spectral interfacial heat current can then be calculated via [18,19,26,27]

$$Q_{L \rightarrow R}(\omega) = \frac{1}{2} \sum_i^L \sum_j^R \text{Re} \left[ \int_{-\infty}^{+\infty} \left\langle \left( \frac{\partial U_{ji}}{\partial \vec{r}_{ji}} - \frac{\partial U_{ij}}{\partial \vec{r}_{ij}} \right) \Big|_{\tau} \cdot [\vec{v}_i(0) + \vec{v}_j(0)] \right\rangle e^{-i\omega\tau} d\tau \right], \quad (2)$$

where  $\tau$  is the correlation time. Meanwhile, it is popular to assume that all the vibrations hold the same temperature drop  $\Delta T$  at interfaces [18,21,22], and the spectral ITC is calculated by

$$G(\omega) = \frac{Q_{L \rightarrow R}(\omega)}{\Delta T}. \quad (3)$$

At the same time, the interfacial heat current can be seen as the couplings among vibrations across the interface [28] and can be calculated by [29,30]

$$Q = \sum_{\omega} \hbar\omega \frac{\partial f(\omega, T)}{\partial T} \Gamma(\omega, T), \quad (4)$$

in which  $f(\omega, T)$  is the equilibrium vibration distribution function following the Bose-Einstein distribution, i.e.,  $f(\omega, T) = [\exp(\hbar\omega/k_B T) - 1]^{-1}$ ,  $k_B$  denotes the Boltzmann constant,  $\hbar$  is the reduced Planck constant,  $\hbar\omega$  is the vibration energy, and  $\Gamma(\omega, T)$  is the vibration transmission function. However, in the classical MD simulations, all the vibrations are inherently fully activated, and the vibration distribution function follows the classical limit of Boltzmann distribution [31,32], i.e.,  $f_{\text{classical limit}}(\omega, T) = \frac{k_B T}{\hbar\omega}$ . Therefore, in the MD simulations, the vibration transmission function becomes [22,31,32]

$$\Gamma(\omega, T) = \frac{Q_{L \rightarrow R}(\omega)}{k_B \Delta T}. \quad (5)$$

The ITC calculated based on NEMD simulations considering the Bose-Einstein distribution of vibrations can then be corrected via [30,33]

$$G^{QC} = \frac{1}{2\pi A} \int_0^{\infty} \hbar\omega \frac{\partial f(\omega, T)}{\partial T} \Gamma(\omega, T) d\omega. \quad (6)$$

To further quantitatively characterize the contribution to ITC from elastic and inelastic vibration scatterings, we regard the vibration transmission function at extremely low

temperatures (e.g., 2 K for the Ar/h-Ar system) as the elastic vibration transmission function (Appendix B). Therefore, the elastic ITC  $G^{\text{ela}}$  can be calculated by substituting the elastic vibration transmission function  $\Gamma^{\text{ela}}(\omega)$  into Eq. (6). This assumption has been validated by comparing the ITC calculated using Eq. (6) with the ITC computed using the original NEGF [17,26]. The corresponding ITC resulting from inelastic vibration scatterings is then obtained by  $G^{\text{inela}} = G^{\text{QC}} - G^{\text{ela}}$

### B. Quantifying the elastic and inelastic interfacial thermal transport based on VDOS similarity and interfacial anharmonicity ratio

It is popular to apply the DMM, which considers the diffuse elastic scatterings at the interface [2,34–37] to evaluate the elastic vibration transmission. The predicted ITC based on the DMM agrees reasonably with the measured ITC when the anharmonicity is negligible (e.g., at low temperatures) [7,38,39]. It can be deduced that the elastic vibration transmission should be strongly related to the VDOS of two contact sides [16,21,37,40,41]. Here, a dimensionless parameter, i.e., the K-L divergence value [42], is introduced to quantify the similarity of VDOS of two contact sides. The K-L divergence value of an interfacial structure with two contact sides is calculated as

$$D_{K-L}(P \parallel Q) = \sum_{\omega} P(\omega) \log_{10} \left[ \frac{P(\omega)}{Q(\omega)} \right], \quad (7)$$

in which  $P(\omega)$  and  $Q(\omega)$  are the normalized VDOS of the two contact sides. Here, the normalized VDOS of two contact sides is calculated using the vibrations of the local interfacial region. It is noted that K-L divergence is a nonsymmetric metric that measures the relative entropy or difference in information represented by two normalized distributions, e.g., the normalized VDOS in our calculations. As shown in Eq. (7), the K-L divergence is always nonnegative, and it can be  $>1$  if the two distributions are significantly different from each other. For instance, our results show that the K-L divergence of VDOS of the Ar/h-Ar interface with a mass ratio of 4 is  $>1$ , which is because the cutoff frequency for Ar and h-Ar are 1 and 2 THz, respectively. A larger K-L divergence value denotes a smaller overlap and a smaller similarity between the two normalized VDOSs. It is noted that, for the weakly bonded interfaces, the interfacial VDOS can be approximated by the bulk VDOS of two counterparts which is used to calculate the vibrational transmission coefficient in the DMM. Meanwhile, the DMM can only consider the elastic scatterings. Therefore, for weakly bonded interfaces with a small K-L divergence (i.e.,  $<0.2$ ), the result calculated based on NEMD simulations agrees well with the DMM predictions since the corresponding ITC is mainly contributed by elastic scatterings, and the interfacial VDOS can be approximated by the bulk VDOS of two counterparts. Our calculations in Appendix C clearly show that the vibrational transmission calculated based on NEMD simulations can be compared with the DMM predictions for these weakly bonded interfaces with a K-L divergence  $<0.2$  [Fig. 1(c)].

At the same time, previous studies [8,10,18,21,22,25,26] have shown that inelastic vibration scatterings may largely

benefit interfacial thermal transport. In bulk crystals, inelastic vibration scatterings are determined by the anharmonicity [44–48]. As discussed in Sec. II A, the inelastic interfacial heat current is determined by the anharmonic part of the atomic potential partial function  $\partial U_{ij}/\partial \vec{r}_{ij}$  and atomic velocity  $\vec{v}_i$ . Therefore, it is easy to know that the inelastic vibration scatterings at interfaces should also be relevant to the anharmonicity of the interfaces. Here, we propose a dimensional parameter, i.e., IAR, based on the anharmonic interatomic force, which is inspired by the anharmonic atomic force defined by Knoop *et al.* [49,50], to quantify the anharmonicity of interfaces.

The atomic potential partial function  $\partial U_{ij}/\partial \vec{r}_{ij}$  in Eq. (1) involving two atoms of two contact sides around the interface can be approximated via

$$\frac{\partial U_{ij}}{\partial r_{ij}^{\alpha}} \approx \sum_{\beta} k_{ij}^{\alpha\beta} (u_j^{\beta} - u_i^{\alpha}), \quad (8)$$

in which  $k_{ij}^{\alpha\beta} = \left. \frac{\partial U_{ij}}{\partial u_j^{\beta} \partial u_i^{\alpha}} \right|_{|\vec{u}|=0}$  is the interfacial second-order force constant, and therefore, we calculate the forces as  $F_{ij}^{\alpha} = k_{ij}^{\alpha\beta} (u_j^{\beta} - u_i^{\alpha})$ . Here, we use the finite displacement method (FDM) to calculate  $k_{ij}^{\alpha\beta}$  with a displacement of  $u_j^{\alpha,\beta,\gamma} = 0.01 \text{ \AA}$ . It is noted that the atomic displacement inherently includes the temperature effects and then the interfacial anharmonicity. In our calculations, the interfacial forces as well as the average forces are calculated based on these atomic trajectories which are output from the MD simulations. The calculation details can be found in Appendix D. We find that the average force increases with temperatures [Fig. 2(a)]. During MD simulations,  $\vec{F}_{ij}$  can be further characterized by the probability density function:

$$p(F) = \frac{1}{3N_t N_{(i,j)}} \sum_t \sum_{(i,j)} \sum_{\alpha} \delta(F - F_{ij}^{\alpha}), \quad (9)$$

where  $\delta(F)$  is the delta distribution. To reduce the computational cost, we only include these atom pairs  $(i, j)$  with a relative distance smaller than the cutoff distance ( $r_{ij} \leq r_{\text{cutoff}}$ , where  $r_{\text{cutoff}}$  denotes the cutoff distance of the interatomic pair potential) in Eq. (9). It is noted that the average value of individual force components [Eq. (8)] should be zero, as atoms vibrate around their equilibrium sites. The width of the interfacial interatomic force distribution function [Eq. (9)] can be evaluated by its standard deviation:

$$\sigma[F] = \sqrt{\int_{-\infty}^{+\infty} F^2 p(F) dF} = \sqrt{\frac{1}{3N_{(i,j)}} \sum_{(i,j)} \sum_{\alpha} \langle F_{ij}^{\alpha} \rangle}, \quad (10)$$

in which  $\langle \rangle$  denotes the time average in MD simulations. Here,  $\sigma[F]$  can be regarded as the average magnitude of interfacial interatomic forces acting on the interfacial thermal transport. Moreover,  $\sigma[F]$  can be regarded as a general scale in which the interfacial interatomic force is given and compared via the *normalized interfacial interatomic forces*, i.e.,  $F_{ij}^{\alpha}(t) \rightarrow F_{ij}^{\alpha}(t)/\sigma[F]$  (Appendix D). Therefore,  $\sigma[F]$  can be calculated by independent EMD simulations with a small system (Appendix D).

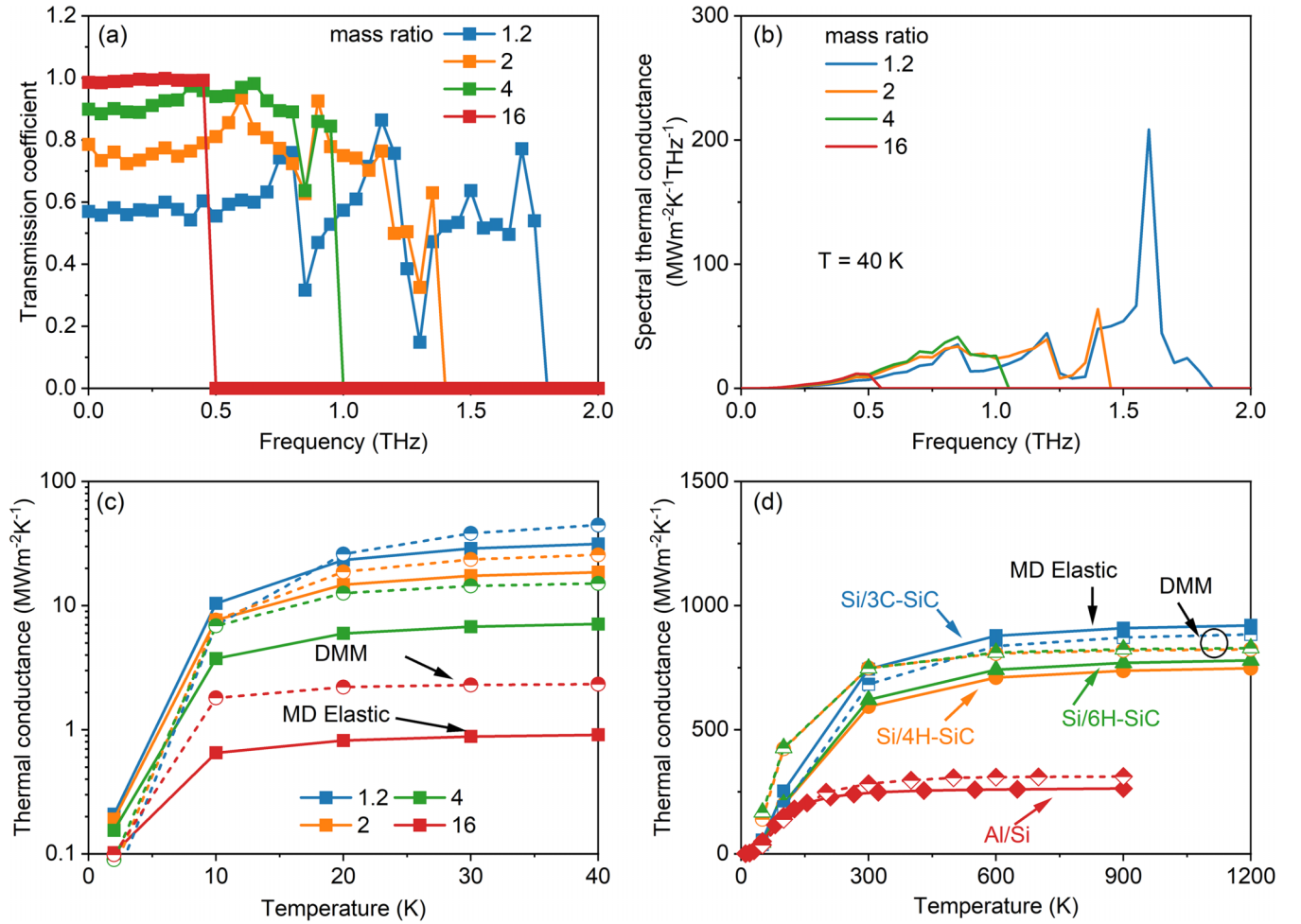


FIG. 1. (a) The transmission coefficient [Eq. (C1)] for Ar/h-Ar interfaces with a mass ratio changing from 1.2 to 16, and (b) the corresponding spectral thermal conductance [Eq. (C2)] of Ar/h-Ar interfaces at  $T = 40$  K. (c) The thermal conductance of Ar/h-Ar interfaces calculated using the diffuse mismatch model (DMM; dash lines) and the elastic thermal conductance (solid lines) computed based on Eq. (6). Here, we apply the same interfacial adhesion parameter ( $\varepsilon_{12} = 0.25\varepsilon$ ) to depict all the Ar/h-Ar interfaces. (d) The elastic thermal conductance of Si/3C-SiC, Si/4H-SiC, Si/6H-SiC, and Al/Si interfaces, adopted from Refs. [22,43].

Specifically,  $\sigma[F]$  at extremely low temperatures (Appendix B), in which the elastic vibration scatterings dominate the interfacial thermal transport [22,26], can be regarded as the harmonic average interfacial interatomic force  $\sigma^{\text{har}}[F]$ . Therefore, a dimensionless parameter IAR can be defined as

$$\text{IAR}(T) = 1 - \frac{\sigma^{\text{har}}[F]}{\sigma[F]_T}, \quad (11)$$

where IAR ranges from 0 to 1 and can be applied to describe the anharmonicity of an interfacial region.

### III. RESULTS AND DISCUSSIONS

#### A. Influence of VDOS similarity between two contacted bulk materials on interfacial thermal transport

It is known that the ITC calculated by the DMM [2,7,25,34–36,39] is determined by the coupling of the VDOS between two contact bulk materials. The ITC calculated using the DMM agrees well with the experimental measurements for these interfaces, in which the interfacial thermal transport

is dominated by elastic scatterings [7–9,36]. Therefore, it is easy to deduce that the elastic scatterings and their contributions to ITC should be strongly correlated with the similarity of the VDOS between two contact bulk materials. To clarify the effect of the VDOS similarity between two contact bulk materials on the elastic contribution to the corresponding ITC, we designed an Ar/h-Ar interface with a mass ratio changing from 1.2 to 16. At the same time, a weak interfacial interaction (i.e.,  $\varepsilon_{12} = 0.25\varepsilon$ ) is chosen to describe the interatomic interactions between two contacted bulk materials. It is noted that, for a weakly bonded interface, the VDOS of the near interface region is like that of its bulk counterpart [37,40] (Appendix E). In this circumstance, the vibration transmission calculated from NEMD can be compared with the DMM predictions (Appendix C).

Our results show that the cutoff frequency of h-Ar decreases when its mass increases and the corresponding overlap of the VDOS between h-Ar and Ar reduces [Fig. 3(a)]. Furthermore, the ITC contributed by the elastic vibration scatterings is found to decrease with the overlap of the VDOS between two contacted leads [Fig. 3(b)]. The elastic vibration

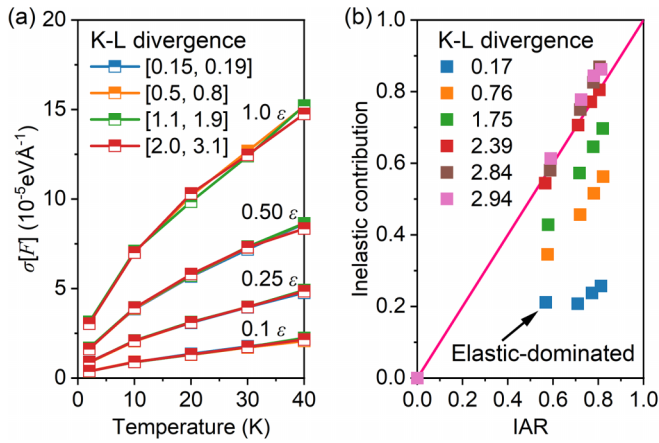


FIG. 2. (a) The average forces  $\sigma[F]$  [Eq. (10)] of interfacial atoms with various interfacial bonding strengths ranging from  $\varepsilon_{12} = 0.1\varepsilon$  to  $1\varepsilon$ . The Kullback-Leibler (K-L) divergence values here are calculated using the vibrational density of states (VDOS) of the interfacial atoms and will change with the interfacial bond strength, as discussed in Sec. III B. We give the range of the K-L divergence here. (b) The inelastic contributions to the total interfacial thermal conductance (ITC) assessed using the interfacial anharmonic ratio (IAR) [Eq. (11)]. For all the Ar/h-Ar interfaces in (b), the interfacial adhesion parameter  $\varepsilon_{12} = 0.25\varepsilon$  is used.

scatterings at the interface should satisfy the energy conservation law, i.e.,  $\omega_1 = \omega_2$ , where  $\omega_1$  and  $\omega_2$  are the incident and transmitted vibration frequencies at two sides. Therefore, a larger overlap of the VDOS between two contacted leads would provide a greater likelihood of finding vibration modes that satisfy  $\omega_1 = \omega_2$  for these elastic scatterings. For example, when the mass difference of the Ar/h-Ar system changes from 1.2 to 16, the maximum frequency of these vibrations contributed to the interfacial thermal transport at a low temperature of 2 K varies from  $\sim 2$  to 0.5 THz [Fig. 3(c)]. We further find that the ITC is mainly contributed by elastic vibration scatterings for the Ar/h-Ar system with a mass ratio of 1.2 even at a temperature of 40 K [Fig. 3(c)]. For the Ar/h-Ar system with a mass ratio of 16, which indicates a large difference of the VDOS between two contacted leads, only these vibrations with frequencies  $< 0.5$  THz can elastically transport thermal energy across the corresponding interface owing to the energy conservation rule [Fig. 3(a)]. Therefore, even at a relatively low temperature of 10 K, the elastic vibration scatterings contribute only 40% of the total ITC [Figs. 3(b) and 3(c)], with the rest contributed by inelastic vibration scatterings.

We further apply the K-L divergence value [Eq. (7)] to quantitatively characterize the similarity of the VDOS of the near-interfacial region [Fig. 4(a)] and attempt to figure out its relationship with the ITC contributed by elastic vibration scatterings. Our results show that the elastic vibration scatterings contribute  $> 75\%$  to the ITC of Ar/h-Ar interfaces with K-L divergence values  $< 0.2$  [Fig. 4(b)]. We also designed an h-Ar/h-Ar grain boundary with a K-L divergence of zero, in which the interfacial bond strength is 0.25 times the bond strength in two contacted bulk leads. We find that the elastic vibration scatterings contribute  $> 90\%$  to the ITC

for the h-Ar/h-Ar grain boundary at all the temperatures considered here [Fig. 4(b)]. Meanwhile, for these interfaces with K-L divergence values  $> 1$ , which indicates a large mismatch of the VDOS between two contacted leads [Figs. 3(a) and 4(b)], elastic vibration scatterings contribute  $< \sim 50\%$  to the corresponding ITC [Fig. 4(b)]. Other interfaces with large K-L divergence values  $> 1$  such as Pt/diamond [10], Si/Al [22], and Si/Ge interfaces [21] also show that both elastic and inelastic vibration scatterings contribute largely to the ITC, e.g., inelastic vibration scatterings contribute  $> 50\%$  to the total ITC for Si/Ge interfaces at room temperature [21]. It is also noted that, for the weakly bonded interface, the K-L divergence value of the near-interfacial region may also be estimated using the VDOS of two contacted bulk counterparts (Appendix E).

### B. Effect of interfacial strength between two contacted leads on thermal transport across interfaces

Meanwhile, it is known that the interfacial strength between two contacted leads will strongly influence the VDOS of atoms near the interface [23,41,51–57]. The VDOS of atoms near the interface may not be approximated by the VDOS of their bulk counterpart (Appendix E). The VDOS or the K-L divergence value of the interface is changed by the interfacial adhesion, which may alter the elastic and inelastic interfacial transmission.

Here, we first change the interfacial interaction of the Ar/h-Ar interface with a fixed mass ratio of 1.2 from  $0.1\varepsilon$  to  $0.75\varepsilon$ . The K-L divergence value is  $< 0.2$  for all Ar/h-Ar interfaces with a mass ratio of 1.2 and decreases with the interfacial interaction (Appendix E). As we discussed above, the interfaces with K-L divergence values  $< 0.2$  indicate a high similarity of the VDOS between two contacted leads. Therefore, the ITC of Ar/h-Ar interfaces with a mass ratio of 1.2 should be mainly contributed by elastic vibration scatterings based on the analysis in Sec. III A. For Ar/h-Ar interfaces with a mass ratio of 1.2, our results show that the elastic vibration scatterings contribute  $\sim 75\%$  to the ITC of these Ar/h-Ar interfaces at all temperatures when two contacted leads are bonded by a weak interfacial interaction of  $0.1\varepsilon$  and  $0.25\varepsilon$  [Fig. 5(a)]. When the interfacial interaction of Ar/h-Ar interfaces becomes  $0.50\varepsilon$  and  $0.75\varepsilon$ , elastic scatterings contribute even 88 and 85% to the ITC at 40 K [Fig. 5(a)], respectively. This is because the strong interfacial interaction can change the local atomic environment, such as interatomic forces and local strain at the interfacial region, which in turn increases the similarity of the VDOS of the local atoms in two contact leads (Appendix E). Therefore, the ITC contributed by the elastic vibration scatterings for these interfaces with a high similarity is still dominant and increases when the interfacial interaction between two contacted leads increases. We further find that the K-L divergence of 0.2 may be applied to distinguish these interfaces with ITCs dominantly contributed from elastic vibration scatterings (i.e.,  $> 70\%$ ). For instance, for Ar/h-Ar interfaces with a K-L divergence of 0.15, the elastic vibration scatterings contribute  $> 85\%$  to the ITC even at 40 K [Figs. 5(a) and 5(b)].

It should be noted that, for these Ar/h-Ar interfaces with large mass ratios, the increase of interfacial interaction may

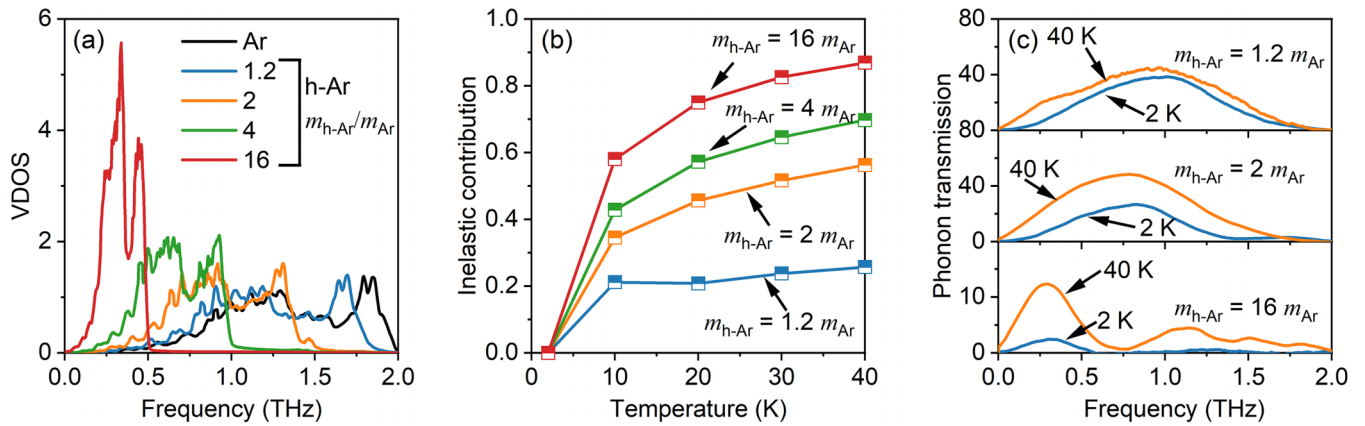


FIG. 3. (a) Vibrational density of states (VDOS) of Ar and h-Ar with various atomic masses, e.g., the mass of h-Ar changes from 1.2 to 16 times that of Ar. (b) The inelastic contribution to the interfacial thermal conductance (ITC) of Ar/h-Ar interfaces with various atomic mass ratios. The inelastic contribution increases with the mass difference, which indicates less overlap of the VDOS. (c) The vibrational transmission function of three selected Ar/h-Ar interfaces, i.e., elastic scattering-dominated interfaces ( $m_{h-Ar} = 1.2 m_{Ar}$ ), inelastic scattering-dominated interfaces ( $m_{h-Ar} = 16 m_{Ar}$ ), and interfaces with comparable contributions from elastic and inelastic scatterings (e.g.,  $m_{h-Ar} = 2 m_{Ar}$ ). For all Ar/h-Ar interfaces considered here, the interfacial bond strength  $\varepsilon_{12} = 0.25\varepsilon$  is applied to depict the interatomic interactions.

decrease the corresponding K-L value from a value  $> 1$  to that  $< 1$ . For instance, for an Ar/h-Ar interface with a mass ratio of 3, the K-L divergence value changes from 1.47 to 0.88 when interfacial adhesion increases from  $0.1\varepsilon$  to  $1.0\varepsilon$ . If an interface has a K-L divergence value  $> 1$ , the ITC contributed by elastic and inelastic vibration scatterings can be assessed based on the IAR (see detailed discussions below). However, for interfaces with K-L divergence values between 0.2 and

1, both elastic and inelastic vibration scatterings contribute largely to the corresponding ITC, and their contributions are challenging to quantify accurately.

### C. The role of interfacial anharmonicity in thermal transport across interfaces

As discussed above, the similarity of the VDOS between two contacted leads is low when the K-L divergence value of interfaces is  $> 1$ . Only a small part of vibrations with frequencies lower than the cutoff frequency of the contacted leads can transfer thermal energy across the interfaces via elastic scatterings based on the energy conservation rule [Fig. 3(a)]. These vibrations with frequencies larger than the cutoff frequency of the contacted leads can only transport ther-

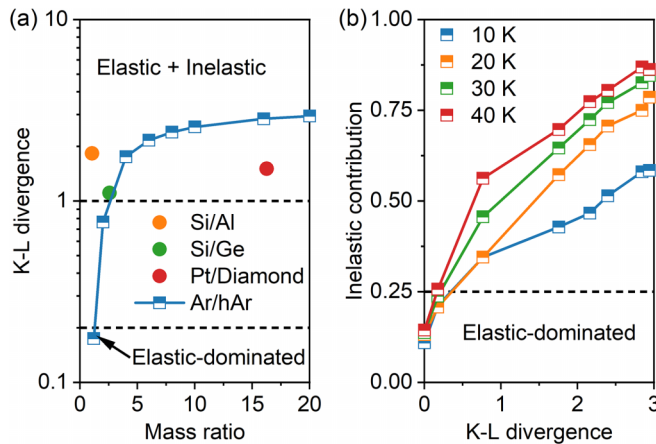


FIG. 4. (a) The Kullback-Leibler (K-L) divergence values [Eq. (7)] of Ar/h-Ar interfaces, with mass ratio changing from 1.2 to 20, and Si/Al and Si/Ge interfaces. The K-L divergence values of Si/Al and Si/Ge interfaces are calculated based on the results of Xu *et al.* [22] and Feng *et al.* [21], respectively. The K-L divergence value of the Pt/diamond interface is calculated based on measurements of Hohensee *et al.* [10]. (b) The ratio of interfacial thermal conductance (ITC) contributed by inelastic scatterings for Ar/h-Ar interfaces with various K-L divergence values. For all Ar/h-Ar interfaces considered here, the interfacial bond strength  $\varepsilon_{12} = 0.25\varepsilon$  is applied to depict the interatomic interactions. We also consider the ideal interface with a K-L divergence value of zero, i.e., h-Ar/h-Ar interfaces with weak interfacial bonds  $\varepsilon_{12} = 0.25\varepsilon$ .

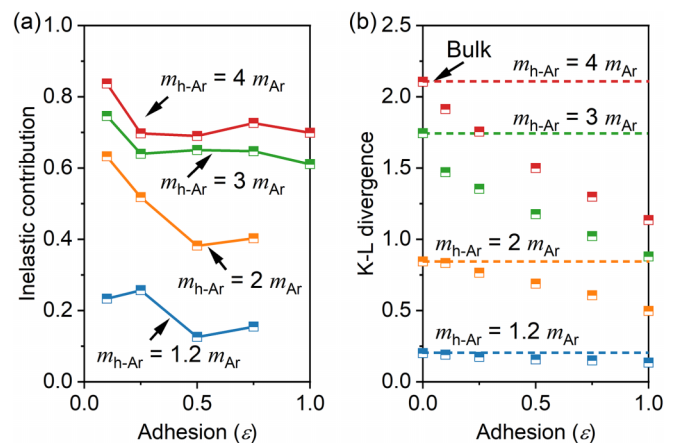


FIG. 5. (a) The inelastic contribution to the total interfacial thermal conductance (ITC) for Ar/h-Ar interfaces with various bonding strengths at  $T = 40$  K. (b) The corresponding Kullback-Leibler (K-L) divergence values calculated using the vibrational density of states (VDOS) of atoms in the interfacial region. The K-L divergence values decrease with the interfacial bonding strength.

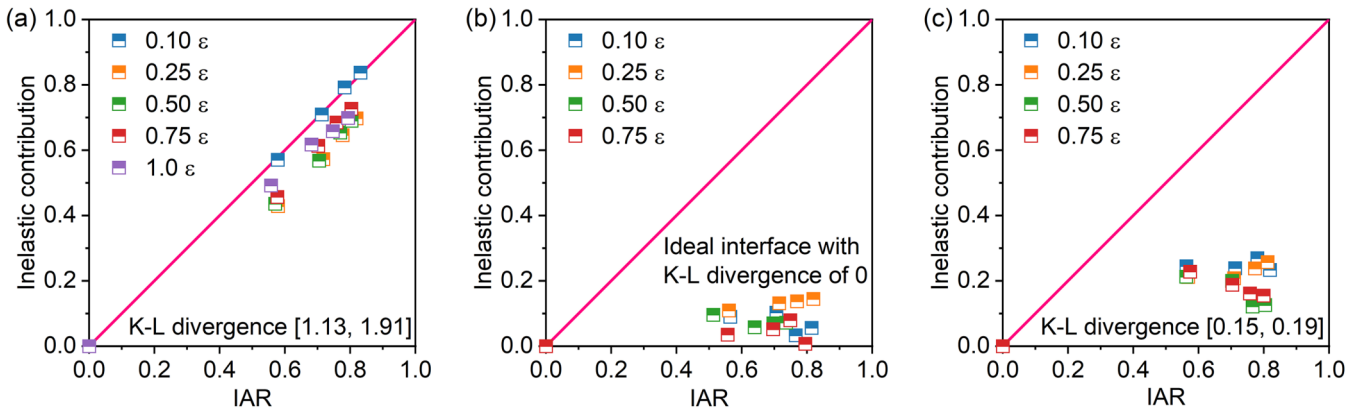


FIG. 6. The influence of the similarity of the vibrational density of states (VDOS) between two contacted leads and the interfacial anharmonicity on the interfacial thermal transport. The Ar/h-Ar interfaces with Kullback-Leibler (K-L) divergence values of (a) [1.13, 1.91], (b) 0, and (c) [0.15, 0.19], considering various interfacial bond strengths. All results here are calculated from  $T = 2$  to 40 K.

mal energy across the interfaces through inelastic scatterings [Fig. 3(a)].

For these interfaces with K-L divergence values  $>1$ , our results show that both elastic and inelastic vibration scatterings contribute largely to the ITC [Fig. 4(b)]. At the same time, the ITC contributed from inelastic vibration scatterings is correlated with the interfacial anharmonicity which is included in the interfacial interatomic forces [17]. To quantify the interfacial anharmonicity, we then calculate the average interfacial interatomic force  $\sigma[F]$  (Appendix D) and find that  $\sigma[F]$  increases with temperature [Fig. 2(a)] as expected. The IAR, which can be used to measure the interfacial anharmonicity, is then obtained using Eq. (11).

Our results show that the IAR of these interfaces with K-L divergence values  $>1$  change almost linearly with the ratio of ITC contributed by inelastic vibration scatterings [Figs. 2(a) and 6(a)]. Therefore, it is suitable to use IAR to quantify the ratio of ITC contributed by inelastic vibration scatterings. However, the ratio of ITC resulting from inelastic vibration scatterings assessed based on IAR will be overestimated when

the K-L divergence value of the interfaces is  $<1$  [Fig. 2(b)]. This is because the IAR only considers the interfacial anharmonicity while ignoring the coupling of the VDOS of two contacted leads. For instance, the calculated IAR at 10 K is 0.57 for Ar/h-Ar interfaces with a K-L divergence value of 0.76, which is much larger than the ratio of ITC contributed by inelastic vibration scatterings [i.e., 35%, Fig. 2(b)]. The IAR is calculated based on the average force  $\sigma[F]$  of the atoms in the interfacial region, which quantifies the overall anharmonicity resulted from these interfacial atoms. It is shown that the IAR contributed by the low-frequency vibrational modes should be generally smaller than that of the high-frequency vibrational modes [50]. Meanwhile, for interfaces with small K-L divergence values, e.g., Ar/h-Ar interfaces with a mass ratio of 1.2 and a K-L divergence value  $<0.2$ , the elastic vibration scatterings which include the specular transmission [37,58] of low-frequency vibrations ( $<1$  THz) can contribute largely to the interfacial thermal transport [Fig. 3(c)]. However, these vibrations contribute a little to the IAR [50] and lead to an overestimation of the contribution to ITC from inelastic scatterings assessed using the IAR.

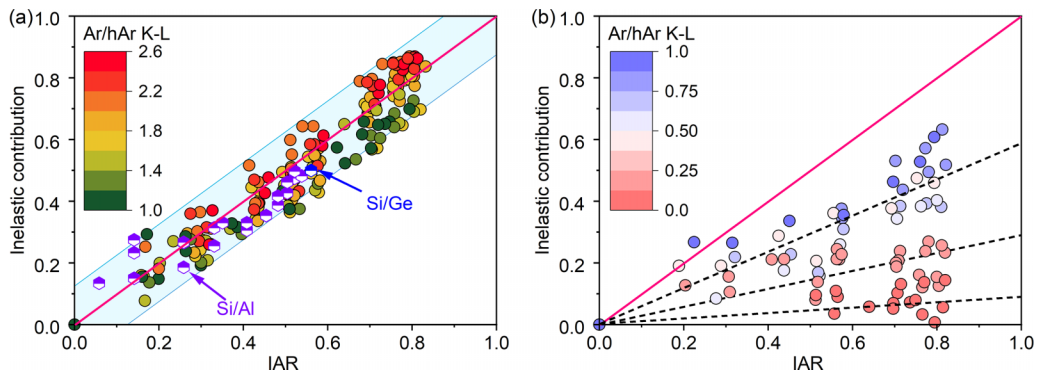


FIG. 7. The inelastic contribution to interfacial thermal transport assessed based on the interfacial anharmonic ratio (IAR) across interfaces with Kullback-Leibler (K-L) divergence values (a)  $>1$  and (b)  $<1$ . The results of Si/Al (from 30 to 900 K) and Si/Ge (300 K) interfaces are reproduced from Refs. [21,22]. The temperatures for Ar/h-Ar interfaces range from 2 to 40 K, with interfacial bonding strength  $\varepsilon_{12}$  changing from  $0.1\varepsilon$  to  $1.0\varepsilon$ . The shadow region in (a) represents the uncertainty ( $\pm 12.5\%$ ) for linearly fitting the inelastic contribution to the total interfacial thermal conductance (ITC) with IAR. The K-L divergence values here are calculated using the vibrational density of states (VDOS) of interfacial atoms (Appendix E).

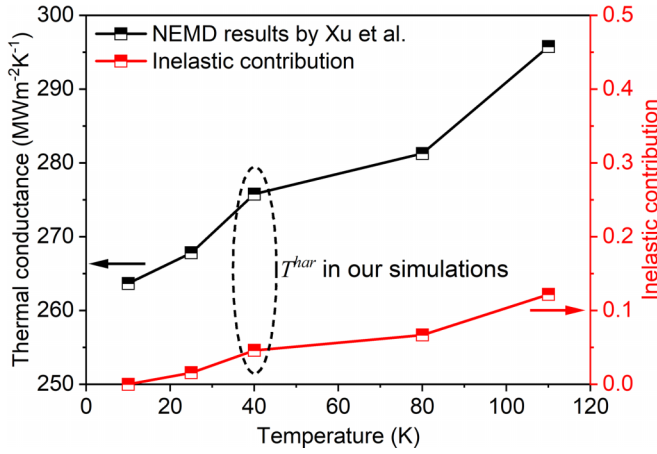


FIG. 8. The interfacial thermal conductance (ITC) of Si/Al interfaces calculated using nonequilibrium molecular dynamics (NEMD) simulations by Xu *et al.* [22]. The interfacial inelastic scatterings at  $T \leq 40$  K contributed  $<5\%$  to the total ITC of Si/Al interfaces, suggesting that interfacial inelastic scatterings at  $T \leq 40$  K could be ignored. Therefore, we chose the average force of Si/Al interfaces at 40 K as the harmonic one  $\sigma^{\text{har}}$  [F] in our simulations.

Consequently, the IAR can be applied to estimate the contribution to ITC from inelastic vibration scatterings for those interfaces with large K-L divergence values (e.g.,  $>1$  for all the interfaces considered here [Figs. 2(b) and 6(b)]). At the same time, the ITC is mainly contributed by elastic vibration scatterings for these interfaces with K-L divergence values  $<0.2$  [Figs. 6(b) and 6(c)] at almost all the temperatures considered here.

#### IV. GENERALIZED DESCRIPTOR FOR QUANTIFYING THERMAL TRANSPORT ACROSS INTERFACES

Overall, the significance of elastic and inelastic vibration scatterings at the interfaces on the interfacial thermal transport

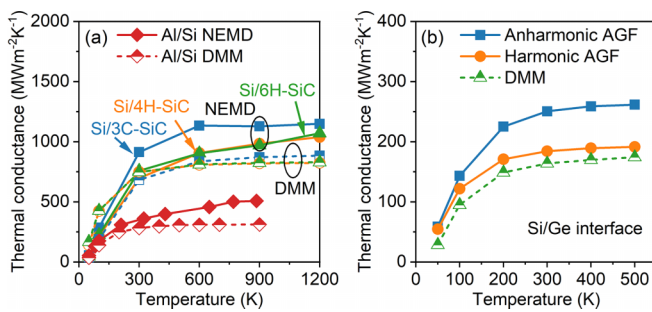


FIG. 9. (a) The thermal conductance of Si/3C-SiC, Si/4H-SiC, Si/6H-SiC, and Al/Si interfaces calculated using nonequilibrium molecular dynamics (NEMD) simulations with quantum correction (QCs) and the diffuse mismatch model (DMM), respectively. The NEMD results here are adopted from Refs. [22,43], respectively. (b) Thermal conductance of the Si/Ge interface predicted by anharmonic atomistic Green's function (AGF) [11] and DMM calculations. The AGF results here are adopted from Ref. [11]. The harmonic AGF considers the elastic scatterings only and agrees well with the DMM estimations.

is determined by the competition between the similarity of the VDOS between two contacted leads and the anharmonicity of the interface, which is characterized by the K-L divergence value and IAR, respectively.

To further validate the accuracy of the measures (i.e., the K-L divergence value and IAR), we include 40 Ar/h-Ar systems with mass ratios ranging from 1.2 to 20 and interfacial interaction ranging from  $0.1\epsilon$  to  $1.0\epsilon$  at temperatures ranging from 2 to 40 K, Si/Al interfaces at temperatures ranging from 30 to 900 K [22], and Si/Ge interfaces at 300 K [21]. For these interfaces with K-L divergence values  $>1$ , which indicates a small VDOS similarity between two contacted leads, the ratios of the elastic and inelastic contributions to ITC can be well characterized by the IAR [Fig. 7(a)]. For instance, for the Ar/h-Ar interfaces with the K-L divergence in range of [1.1, 1.9], IAR estimates that the ratio of ITC contributed by inelastic vibration scatterings is from  $\sim 20$  to  $\sim 80\%$  when the temperature ranges from 3 to 40 K. The predictions based on IAR agree well with the results calculated using MD simulations, which show that the ratio of elastic contribution to ITC is from  $\sim 17$  to  $\sim 80\%$  [Fig. 7(a)]. However, the IAR fails to predict the ratio of contributions of the elastic and inelastic scatterings to ITC for these interfaces with high VDOS similarities between two contacted leads (i.e., the corresponding K-L divergence value is  $<1$ ). This is because the high VDOS similarity between two contacted leads can lead to a large contribution to ITC from elastic scattering channels. For example, for the Ar/h-Ar interfaces with the K-L divergence value of  $<0.2$ , elastic vibration scatterings contribute  $>80\%$  to the ITC at temperatures ranging from 10 to 40 K, much lower than predicted using IAR. For these interfaces with K-L divergence values ranging from 0.2 to 1, both the interfacial anharmonicity and the similarity of VDOS between two contacted leads largely affect the interfacial thermal transport. The ratio of the ITC contributed by inelastic vibration scatterings at these interfaces can neither be ignored nor solely estimated using IAR [Fig. 7(b)]. Moreover, we validate these two metrics by considering higher temperatures and including more systems (Appendix F), and our results show that these metrics depict the effect of the elastic and inelastic vibrational scatterings on interfacial thermal transport well.

#### V. CONCLUSIONS

In conclusion, we have systematically quantified the contributions to ITC from elastic and inelastic vibration scatterings using NEMD simulations, VDOS, and interfacial interatomic force analysis. Our results show that the ratio to ITC resulting from elastic and inelastic vibration scatterings is determined by the competition between the VDOS similarity between two contacted leads and the anharmonicity of the interface. We further propose two measures, i.e., the K-L divergence value and IAR, to quantify the similarity of the VDOS between two contacted leads and interfacial anharmonicity, respectively. Our results show that the ITC across interfaces is dominated by elastic vibration scatterings when the K-L divergence values are  $<0.2$ , e.g., the elastic vibration scatterings contribute  $>80\%$  to the ITC for these Ar/h-Ar interfaces with a K-L divergence value of 0.19. For these interfaces with K-L divergence values  $>0.2$ , both elastic and inelastic vibration

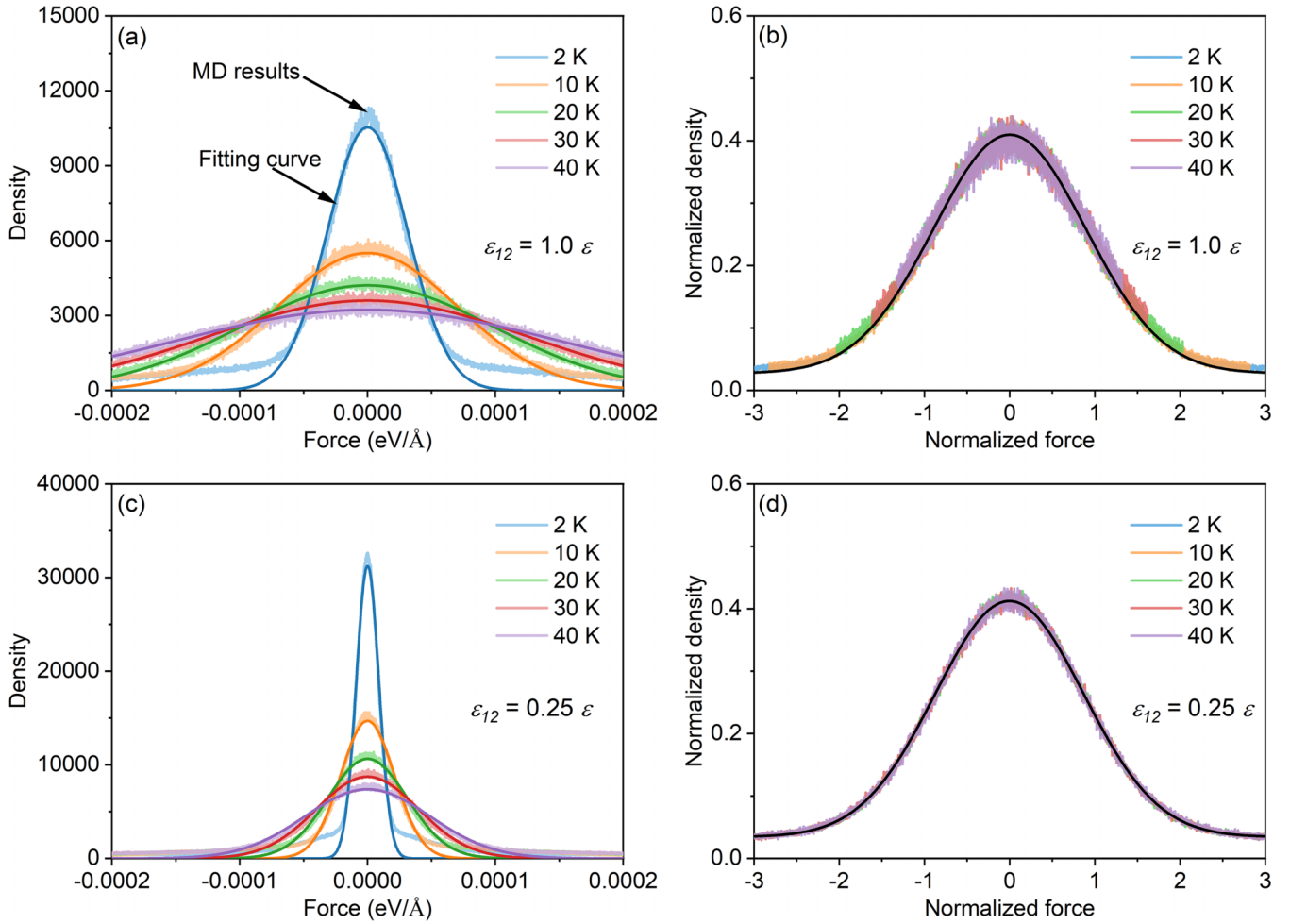


FIG. 10. The distribution functions of interatomic forces between Ar and h-Ar atoms at Ar/h-Ar interfaces with a mass ratio of 4, and the interfacial bonding parameters are (a)  $\varepsilon_{12} = 1.0\varepsilon$  and (c)  $\varepsilon_{12} = 0.25\varepsilon$ , respectively. We also apply the Gaussian function to fit the distribution of interatomic forces. The corresponding normalized distribution function of interatomic forces with interfacial bonding of (b)  $\varepsilon_{12} = 1.0\varepsilon$  and (d)  $\varepsilon_{12} = 0.25\varepsilon$ . The dark lines in (b) and (d) are plotted for view, which shows that the normalized forces at various temperatures and interfacial bonding strengths can be reduced to an identical distribution.

scatterings are found to contribute largely to the ITC. Furthermore, the contributions to ITC from elastic and inelastic vibration scatterings for these interfaces with K-L divergence values  $>1$  can be quantified using a generalized descriptor IAR. Our results on Ar/h-Ar, Si/Al, and Si/Ge interfaces at various temperatures with K-L divergence values  $>1$  show that the IAR is generally linear with the inelastic contribution to ITC with an error of 12.5%. Our results here advance the understanding of determining the contributions to ITC from elastic and inelastic vibration scatterings.

#### ACKNOWLEDGMENTS

Y.Z. acknowledges the startup fund (Grant No. REC20EGR14, a/c-R9246) and Frontier Technology Research for Joint Institutes with Industry Scheme (Grant No. FTRIS-002) from Hong Kong University of Science and Technology (HKUST). Y.Z. acknowledges the fund from the Research Grants Council of the Hong Kong Special Administrative Region under Grants No. C6020-22G, No. 26206023, No. 16207124, and No. C7002-22Y, the fund from

the Guangdong Natural Science Foundation under Grant No. 2024A1515011407. Y.Z. also thanks the Hong Kong SciTech Pioneers Award from the Y-LOT foundation. Y.X. thanks J. Yu for the discussion.

#### APPENDIX A: NEMD SIMULATIONS

In this paper, a typical interfacial structure constructed by two dissimilar Lennard-Jones (LJ) face-centered-cubic lattices, i.e., Ar/h-Ar with a mass ratio ranging from 1.2 to 20, is used to analyze the interfacial thermal transport. The system size is set as  $160a \times 10a \times 10a$ , in which  $a = 5.29 \text{ \AA}$  is the lattice constant at 10 K. In our previous work, we have shown that the system size is large enough to exclude the size effects in the NEMD simulations [26]. The parameters used in the LJ potential  $U_{ij} = 4\varepsilon[(\sigma/r_{ij})^{12} - (\sigma/r_{ij})^6]$  are  $\varepsilon = 0.0104 \text{ eV}$  and  $\sigma = 3.4 \text{ \AA}$  [59]. The cutoff distance for LJ interaction is  $2.5\sigma$ , and the simulation timestep is 1 fs. At the same time, we also considered the interfacial bonding strength in our simulations by changing the interaction between Ar and h-Ar atoms  $\varepsilon_{12}$  from  $\varepsilon_{12} = 1.0\varepsilon$  to  $0.1\varepsilon$ . Periodical boundary

conditions are applied to the lateral directions of the system, i.e., perpendicular to the direction of heat flow. All the MD simulations are performed by LAMMPS [60].

Here, we first relax the system at the NPT (constant particle number, pressure, and temperature) ensemble for 2 ns, in which the pressure is set as 1 bar for all the temperatures. Then the system is relaxed at the NVT (constant particle number, volume, and temperature) ensemble for another 2 ns. After the equilibrium, the system is applied with heat current using the NVE (constant particle number, volume, and energy) ensemble for another 8 ns. The heat current is generated by applying the temperature coupling to the two Langevin thermostats at two ends of the system, i.e.,  $T_{\text{thermostat}} = T \pm 0.5T$ , where  $T$  is the system temperature. It took  $\sim 4\text{--}6$  ns to obtain the steady state (stable temperature distribution and steady system heat current) of the system. Following that, we further run the NEMD simulations for another 2 ns to output the atomic trajectories at the interfacial region (one unit cell length at both sides of the interface) to calculate the spectral interfacial heat current. Meanwhile, the system heat current can also be calculated via  $Q = \langle dE/dt \rangle$ , where  $E$  is the accumulative energy in the thermostats. The ITC can be calculated via Fourier's law  $G = Q/A\Delta T$ , in which  $A$  is the system cross-section area ( $10a \times 10a$ ) and  $\Delta T$  is the temperature drop at the interface, which is calculated by linearly fitting the temperature distribution of Ar and h-Ar lattices.

## APPENDIX B: CRITICAL TEMPERATURE FOR DETERMINING ELASTIC ITC

In the MD simulations, vibrational scatterings may be ignored at extremely low temperatures [32], e.g.,  $T^{\text{har}} < 0.05\theta_D$ , where  $\theta_D$  is the Debye temperature and can be estimated via  $\theta_D = \hbar\omega_{\text{cutoff}}/k_B$ . At such low temperatures ( $T^{\text{har}} < 0.05\theta_D$ ), the corresponding interfacial thermal transport is dominated by the elastic scatterings [22,26,27]. For instance, in our previous work [26], we show the vibration transmission function at 2 K ( $\sim 0.02\theta_D^{\text{Ar}}$ ) of Ar/h-Ar interfaces calculated using NEMD simulations is almost identical to that predicted by the atomistic Green's function (AGF) method, in which the inelastic scatterings are ignored. Therefore, we use the vibration transmission at  $T = 2$  K as the elastic transmission for all the Ar/h-Ar interfaces. At the same time, the harmonic average force  $\sigma^{\text{har}}[F]$  is then calculated at such temperature, e.g.,  $T^{\text{har}} = 2$  K for Ar/h-Ar interfaces in our calculations.

For Si/Al and Si/Ge interfaces, we ignore the inelastic scatterings at 40 K ( $\sim 0.04\theta_D^{\text{Si}}$ ) and regard the average force as the harmonic one  $\sigma^{\text{har}}[F]$ . The corresponding IAR can be then calculated [Fig. 7(a)]. Furthermore, our previous NEMD calculations show that inelastic scatterings at the interface contribute  $\sim 5\%$  to the total ITC at 40 K for Si/Al interfaces (Fig. 8). It is, therefore, reasonable to choose the average force of Si/Al interfaces at 40 K as the harmonic one  $\sigma^{\text{har}}[F]$ .

It is also noted that the temperature range for various sets of interfaces is chosen based on their lower Debye temperatures. For instance, the lower Debye temperatures of the Al/Si and Ar/hAr interfaces are around  $\theta_D^{\text{Al}} = 423$  K and  $\theta_D^{\text{h-Ar}} = 46$  K ( $m_{\text{h-Ar}} = 4m_{\text{Ar}}$ ) [61], respectively. We can assume that all the vibrations within the lower cutoff frequencies are fully activated and involved in the interfacial

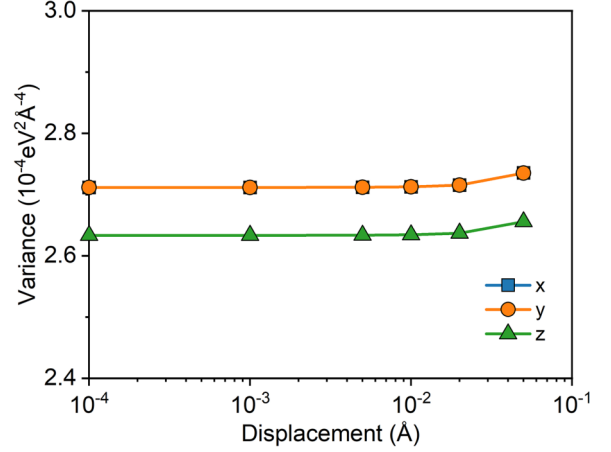


FIG. 11. The variance of force constants  $k_{ij}^{\alpha\beta} = \left. \frac{\partial U_{ij}}{\partial u_j^\alpha \partial u_i^\beta} \right|_{|\vec{u}|=0}$  of the Ar/hAr interfacial structure. The variance is calculated as  $\text{Var} = \frac{1}{N-1} \sum (k_{ij}^{\alpha\beta} - \frac{1}{N} \sum k_{ij}^{\alpha\beta})^2$ . In our simulations, we choose the displacement  $u_j^{\alpha,\beta,\gamma} = 0.01 \text{ \AA}$  to calculate the interfacial force constants.  $x$ ,  $y$ , and  $z$  denote the three directions of the force constants, e.g.,  $x$  includes the  $k_{ij}^{xx}$ ,  $k_{ij}^{xy}$ , and  $k_{ij}^{xz}$  terms in the force constant matrix.

phonon transport. Therefore, the ITC contributed by elastic scatterings converges when temperature increases to the lower Debye temperature. When the system temperature further increases to a value above the lower Debye temperature, e.g.,  $T = 1.5\theta_D$ , phonons with frequencies higher than the lower cutoff frequency are activated and contribute to the ITC via the inelastic scatterings [22,31,32]. Therefore, we set various temperature ranges for various sets of interfaces in our calculations to include all these elastic and inelastic effects on interfacial thermal transport. The temperature range of various sets of interfaces in our calculations ranges from  $T = 0.02\theta_D - 0.04\theta_D$  to  $2\theta_D$ .

## APPENDIX C: DMM

It is known that elastic vibration transmission may be assessed using the DMM [2,34–37]. Here, we also calculate the vibration transmission coefficients at the Ar/h-Ar interface based on the DMM theory [39], which is given by

$$\zeta^{1 \rightarrow 2}(\omega) = \frac{\sum_{\lambda} [k_{\lambda,2}(\omega)]^2}{\sum_{\lambda} [k_{\lambda,2}(\omega)]^2 + \sum_{\lambda} [k_{\lambda,1}(\omega)]^2}, \quad (\text{C1})$$

in which  $\zeta^{1 \rightarrow 2}$  denotes the vibration transmission from side 1 (Ar) to side 2 (h-Ar) and  $k$  is the wave vector. The ITC of Ar/h-Ar interfaces then becomes

$$G^{\text{DMM}} = \frac{1}{8\pi^2} \sum_{\lambda} \int_{k_{\lambda,1} > 0} \hbar\omega_{\lambda,1}(k_{\lambda,1}) k_{\lambda,1}^2 \zeta^{1 \rightarrow 2} \times |v_{\lambda,1}^{\perp}(k_{\lambda,1})| \frac{\partial f}{\partial T} dk_{\lambda,1}, \quad (\text{C2})$$

where  $v_{\lambda,1}^{\perp}(k_{\lambda,1})$  is the group velocity normal to the interface, and  $f$  is the equilibrium vibration distribution, i.e., the Bose-Einstein distribution. As shown in Fig. 1(a), the DMM largely overestimates the vibration transmission across the Ar/h-Ar interface with a mass ratio of 16, in which all the vibrations

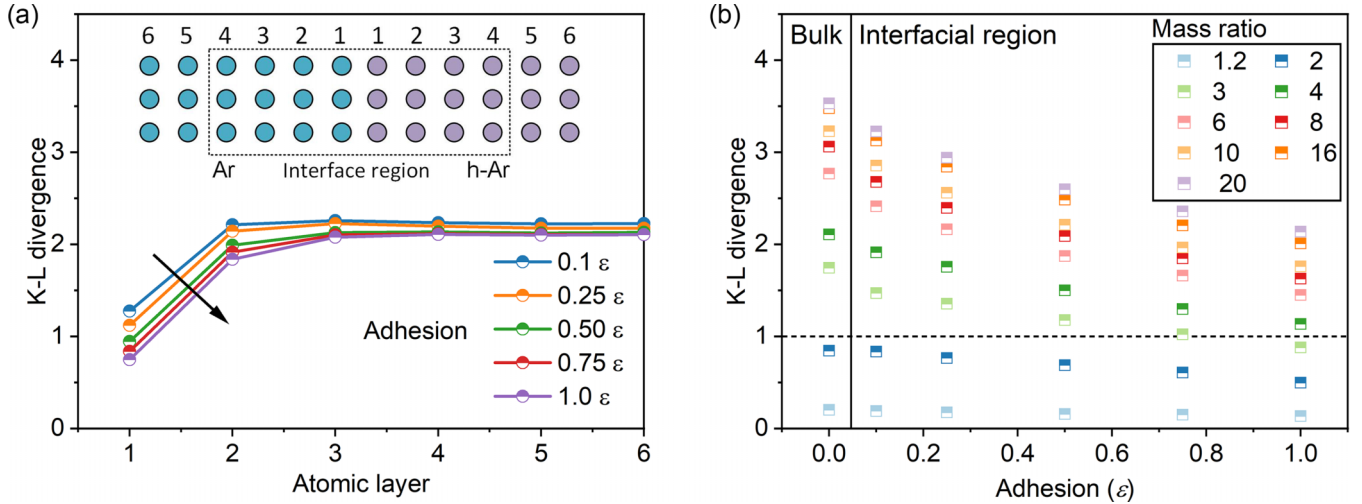


FIG. 12. (a) The Kullback-Leibler (K-L) divergence value which is calculated using the vibrational density of states (VDOS) of the interfacial region with various atomic layers and a mass ratio of 4. (b) The K-L divergence values of the Ar/h-Ar interfaces with various mass ratios.

with a frequency  $<0.5$  THz on the Ar side are assumed to transmit to the h-Ar side fully [Fig. 1(b)]. This is because the DMM only considers the diffusive scatterings but ignores their specular and nonspecular transmission [37,58]. Sadasivam *et al.* [58] have suggested that the specular transmission of low-frequency or long-wavelength vibrations, i.e., the transmitted vibration remains in the same in-plane wave vector, contributes nonnegligibly to the ITC.

On the contrary, the DMM may reasonably depict the Ar/h-Ar interface with a high overlap of the VDOS [e.g., the mass ratio of 1.2 in Fig. 1(c)], in which the contribution to ITC from these low-frequency vibrations is small. For instance, the corresponding transmission function is changed from 1 to 0.6 when the mass ratio decreases from 16 to 1.2 [Fig. 1(a)]. Therefore, the ITC of the Ar/h-Ar interfaces with a high overlap of VDOS or equivalently a small K-L divergence value (e.g., the mass ratio of 1.2) predicted by DMM agrees reasonably with the elastic ITC calculated based on MD simulations [Fig. 1(c)]. Furthermore, the experimental result [8] shows that the diffusive elastic scatterings are the dominant thermal transport channels across the interfaces with a high overlap of VDOS or, equivalently, a small K-L divergence value, such as the Al/GaN interface in which the cutoff frequency of acoustic vibrations for both Al and GaN is  $\sim 10$  THz.

In the meantime, we also examine the ITC of Si/SiC, Si/Ge, and Al/Si interfaces by comparing the DMM calculations with NEMD simulations. Our results show that the DMM underestimates the ITC of Si/3C-SiC, Si/4H-SiC, Si/6H-SiC, Al/Si, and Si/Ge interfaces [Fig. 9(a)]. However, it may reasonably estimate the contribution to ITC resulting from elastic scatterings when most scatterings are diffusive. For instance, the ITC of Si/Ge interfaces predicted using the DMM agrees well with the ITC calculated using the harmonic AGF [11], which only includes elastic scatterings at interfaces [Fig. 9(b)]. The NEMD or AGF results on Ar/h-Ar, Si/3C-SiC, Si/4H-SiC, Si/6H-SiC, Al/Si, and Si/Ge interfaces also show that the DMM can reasonably predict the ITC contributed by elastic scatterings [Figs. 1(d) and 9(b)]. Therefore, for interfaces

with a K-L divergence value  $<0.2$ , such as Al/Si and Si/Ge interfaces, the DMM may be applied to predict the ITC. However, the DMM fails to evaluate the ITC of interfaces with a K-L divergence value  $>0.2$ , where the contribution to ITC from inelastic scatterings is nonnegligible.

#### APPENDIX D: VALIDATION AND CALCULATION OF NORMALIZED FORCES

The IAR is a generalized scale independent of the size of the systems. It is, therefore, reasonable to use a system to calculate the average force  $\sigma[F]$  and the corresponding IAR. Here, the system size to calculate the average force  $\sigma[F]$  of Ar/h-Ar interfaces is set as  $20a \times 4a \times 4a$ , in which the length of Ar and h-Ar leads is  $10a$ . Periodical boundary conditions are applied to the lateral directions of systems. We first relax the system at the NPT ensemble for 4 ns, in which the pressure is set as 1 bar for all the temperatures. Then we perform EMD simulations at the NVE ensemble for 2 ns, during which the atomic displacements of the control volume (i.e., the length is  $2a$ ) at the interfacial region are output every 0.1 ps. It is noted that we only consider the interatomic forces contributed by these atom pairs with  $r_{ij} < r_{\text{cutoff}}$ . The interfacial interatomic force  $\vec{F}_{ij}$  is calculated using the FDM based on these MD trajectories, as discussed in Sec. II B.

As shown in Figs. 10(a) and 10(c), the force distribution function [Eq. (9)] can be calculated based on MD trajectories. The average force  $\sigma[F]$  [Eq. (10)] is then obtained by fitting the force distribution using a Gaussian function. It is noted that the mean value of the individual force components should be zero. Furthermore, we show that the normalized forces, i.e.,  $F_{ij}^\alpha(t) \rightarrow F_{ij}^\alpha(t)/\sigma[F]$ , exhibit the same unit for various systems at different temperatures, e.g., the density function of the normalized forces [Figs. 10(b) and 10(d)] can be reduced to the identical distribution.

Meanwhile, we also validate the accuracy of our interfacial second-order force constants used the FDM. Our results show that a displacement  $u_j^{\alpha,\beta,\gamma} = 0.01 \text{ \AA}$  should be small enough

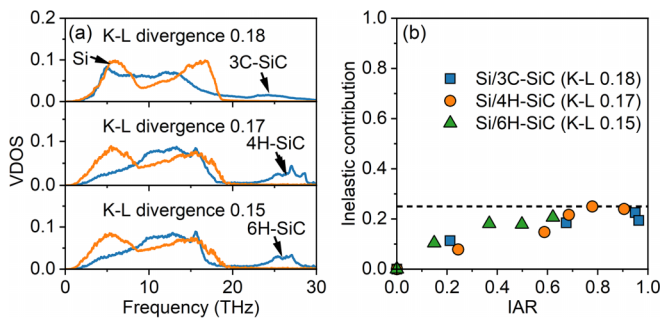


FIG. 13. (a) The vibrational density of states (VDOS) of Si/3C-SiC, Si/4H-SiC, and Si/6H-SiC interfaces and their Kullback-Leibler (K-L) divergences of the interface, respectively. (b) Inelastic contribution to thermal transport of Si/SiC interfaces with temperatures ranging from 50 to 1200 K. The inelastic contribution was adopted from Ref. [43].

to obtain the accurate interfacial second-order force constants (Fig. 11).

#### APPENDIX E: K-L DIVERGENCE VALUES OF REAL INTERFACIAL STRUCTURES

As discussed in Sec. III B, the K-L divergence value of real interfacial structure may differ from the value calculated using their bulk counterparts. We therefore examine all Ar/h-Ar interfaces with a mass ratio changing from 1.2 to 20 and an interfacial adhesion ranging from  $0.1\varepsilon$  to  $1.0\varepsilon$ . We first choose the control volume of the interfacial structures with several layers of interfacial atoms, e.g., four atomic layers at Ar and h-Ar leads (Fig. 12). The size of the control volume is determined by the interatomic forces between interfacial atoms from two contacted leads. The larger control volume contains more atoms of which the VDOS is identical to that of their bulk counterpart [Fig. 12(a)]. These atoms do not directly interact with atoms belonging to the other interfacial side. The corresponding K-L divergence may then be overestimated when a large control volume is used to calculate the value. Here, we choose the control volume to only include these atoms that interact with the other interfacial sides, e.g., four atomic layers at Ar and h-Ar leads, and the interfacial VDOS is calculated based on the atoms in the control volume. Our results show that the K-L divergence value calculated using the real interfacial structure is smaller than that computed using two contacted bulk systems [Fig. 12(b)]. Only for these Ar/h-Ar interfaces with a small mass ratio and a

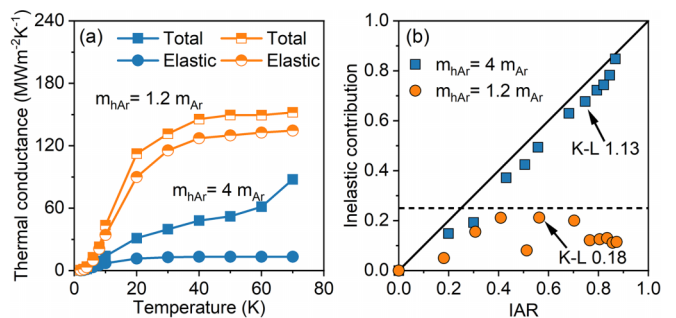


FIG. 14. (a) The thermal conductance of Ar/h-Ar interfaces considering two mass ratios ( $m_{h-Ar} = 1.2m_{Ar}$  and  $4m_{Ar}$ ) with temperature ranging from 2 to 70 K. (b) The corresponding inelastic contribution to the thermal transport across Ar/h-Ar interfaces in (a).

weak interfacial adhesion (e.g., the mass ratio is 1.2, and the interfacial adhesion is  $0.1\varepsilon$ ) may we use the VDOS of two contacted bulk counterparts to calculate the K-L divergence value [Fig. 12(b)].

#### APPENDIX F: VALIDATION OF TWO METRICS AT HIGH TEMPERATURES

We consider three more systems (Si/3C-SiC, Si/4H-SiC, and Si/6H-SiC interfaces) to validate our conclusions on the metric, K-L divergence. As shown in Fig. 13(a), the K-L divergence of the Si/3C-SiC interface is 0.18, indicating that thermal transport across such an interface should be elastic dominated. This is further verified by our finding [Fig. 9(a)] that the results from NEMD simulations with quantum correction agree well with the DMM calculations, in which only the elastic scatterings are included. At the same time, we also show that the IAR fails to describe the inelastic contributions of thermal transport across these Si/SiC interfaces, in which the elastic scatterings contribute  $>75\%$  at even a high temperature of 1200 K [Fig. 13(b)].

We further show that the inelastic contribution of the Ar/h-Ar interface with K-L divergence  $>1$  at high temperatures ( $T > 40$  K) can also be estimated by the IAR. For the interfaces with K-L divergence  $<0.2$ , the inelastic contribution is  $<25\%$  at even high temperatures ( $T > 40$  K for Ar/h-Ar and  $T > 800$  K for Si/SiC interfaces) as shown in Figs. 13 and 14. Therefore, the two metrics we proposed here should be also valid at higher temperatures for these interfaces.

- [1] W. A. Little, The transport of heat between dissimilar solids at low temperatures, *Can. J. Phys.* **37**, 334 (1959).
- [2] E. T. Swartz and R. O. Pohl, Thermal boundary resistance, *Rev. Mod. Phys.* **61**, 605 (1989).
- [3] W. Zhang, T. S. Fisher, and N. Mingo, The atomistic Green's function method: An efficient simulation approach for nanoscale phonon transport, *Numer. Heat Transf. B* **51**, 333 (2007).

- [4] W. Zhang, N. Mingo, and T. S. Fisher, Simulation of phonon transport across a non-polar nanowire junction using an atomistic Green's function method, *Phys. Rev. B* **76**, 195429 (2007).
- [5] L. Yang, B. Latour, and A. J. Minnich, Phonon transmission at crystalline-amorphous interfaces studied using mode-resolved atomistic Green's functions, *Phys. Rev. B* **97**, 205306 (2018).

- [6] J.-S. Wang, J. Wang, and N. Zeng, Nonequilibrium Green's function approach to mesoscopic thermal transport, *Phys. Rev. B* **74**, 033408 (2006).
- [7] C. Hua, X. Chen, N. K. Ravichandran, and A. J. Minnich, Experimental metrology to obtain thermal phonon transmission coefficients at solid interfaces, *Phys. Rev. B* **95**, 205423 (2017).
- [8] Q. Li, F. Liu, S. Hu, H. Song, S. Yang, H. Jiang, T. Wang, Y. K. Koh, C. Zhao, F. Kang *et al.*, Inelastic phonon transport across atomically sharp metal/semiconductor interfaces, *Nat. Commun.* **13**, 4901 (2022).
- [9] R. M. Costescu, M. A. Wall, and D. G. Cahill, Thermal conductance of epitaxial interfaces, *Phys. Rev. B* **67**, 054302 (2003).
- [10] G. T. Hohensee, R. B. Wilson, and D. G. Cahill, Thermal conductance of metal-diamond interfaces at high pressure, *Nat. Commun.* **6**, 6578 (2015).
- [11] J. Dai and Z. Tian, Rigorous formalism of anharmonic atomistic Green's function for three-dimensional interfaces, *Phys. Rev. B* **101**, 041301(R) (2020).
- [12] Y. Guo, Z. Zhang, M. Bescond, S. Xiong, M. Nomura, and S. Volz, Anharmonic phonon-phonon scattering at the interface between two solids by nonequilibrium Green's function formalism, *Phys. Rev. B* **103**, 174306 (2021).
- [13] Y. Guo, M. Bescond, Z. Zhang, M. Luisier, M. Nomura, and S. Volz, Quantum mechanical modeling of anharmonic phonon-phonon scattering in nanostructures, *Phys. Rev. B* **102**, 195412 (2020).
- [14] H. R. Seyf, K. Gordiz, F. DeAngelis, and A. Henry, Using Green-Kubo modal analysis (GKMA) and interface conductance modal analysis (ICMA) to study phonon transport with molecular dynamics, *J. Appl. Phys.* **125**, 081101 (2019).
- [15] K. Gordiz and A. Henry, Phonon transport at interfaces: Determining the correct modes of vibration, *J. Appl. Phys.* **119**, 015101 (2016).
- [16] K. Gordiz and A. Henry, Phonon transport at crystalline Si/Ge interfaces: The role of interfacial modes of vibration, *Sci. Rep.* **6**, 23139 (2016).
- [17] K. Sääskilähti, J. Oksanen, J. Tulkki, and S. Volz, Role of anharmonic phonon scattering in the spectrally decomposed thermal conductance at planar interfaces, *Phys. Rev. B* **90**, 134312 (2014).
- [18] Y. Zhou and M. Hu, Full quantification of frequency-dependent interfacial thermal conductance contributed by two- and three-phonon scattering processes from nonequilibrium molecular dynamics simulations, *Phys. Rev. B* **95**, 115313 (2017).
- [19] Y. Zhou, X. Zhang, and M. Hu, Quantitatively analyzing phonon spectral contribution of thermal conductivity based on nonequilibrium molecular dynamics simulations. I. From space Fourier transform, *Phys. Rev. B* **92**, 195204 (2015).
- [20] Y. Zhou and M. Hu, Quantitatively analyzing phonon spectral contribution of thermal conductivity based on nonequilibrium molecular dynamics simulations. II. From time Fourier transform, *Phys. Rev. B* **92**, 195205 (2015).
- [21] T. Feng, Y. Zhong, J. Shi, and X. Ruan, Unexpected high inelastic phonon transport across solid-solid interface: Modal nonequilibrium molecular dynamics simulations and Landauer analysis, *Phys. Rev. B* **99**, 045301 (2019).
- [22] Y. Xu, H. Fan, Z. Li, and Y. Zhou, Signatures of anharmonic phonon transport in ultrahigh thermal conductance across atomically sharp metal/semiconductor interface, *Int. J. Heat Mass Transf.* **201**, 123628 (2023).
- [23] B. Xu, S. Hu, S.-W. Hung, C. Shao, H. Chandra, F.-R. Chen, T. Kodama, and J. Shiomi, Weaker bonding can give larger thermal conductance at highly mismatched interfaces, *Sci. Adv.* **7**, eabf8197 (2021).
- [24] G. Wang, H. Fan, J. Li, Z. Li, and Y. Zhou, Direct observation of tunable thermal conductance at solid/porous crystalline solid interfaces induced by water adsorbates, *Nat. Commun.* **15**, 2304 (2024).
- [25] J. T. Gaskins, G. Kotsonis, A. Giri, S. Ju, A. Rohskopf, Y. Wang, T. Bai, E. Sachet, C. T. Shelton, Z. Liu *et al.*, Thermal boundary conductance across heteroepitaxial ZnO/GaN interfaces: Assessment of the phonon gas model, *Nano Lett.* **18**, 7469 (2018).
- [26] Y. Xu, L. Yang, and Y. Zhou, The interfacial thermal conductance spectrum in nonequilibrium molecular dynamics simulations considering anharmonicity, asymmetry and quantum effects, *Phys. Chem. Chem. Phys.* **24**, 24503 (2022).
- [27] Y.-X. Xu, H.-Z. Fan, and Y.-G. Zhou, Quantifying spectral thermal transport properties in framework of molecular dynamics simulations: A comprehensive review, *Rare Met.* **42**, 3914 (2023).
- [28] J. Chen, X. Xu, J. Zhou, and B. Li, Interfacial thermal resistance: Past, present, and future, *Rev. Mod. Phys.* **94**, 025002 (2022).
- [29] Y. Imry and R. Landauer, Conductance viewed as transmission, *Rev. Mod. Phys.* **71**, S306 (1999).
- [30] R. Landauer, Spatial variation of currents and fields due to localized scatterers in metallic conduction, *IBM J. Res. Dev.* **1**, 223 (1957).
- [31] J. E. Turney, A. J. H. McGaughey, and C. H. Amon, Assessing the applicability of quantum corrections to classical thermal conductivity predictions, *Phys. Rev. B* **79**, 224305 (2009).
- [32] Y. Zhou, Assessing the quantum effect in classical thermal conductivity of amorphous silicon, *J. Appl. Phys.* **129**, 235104 (2021).
- [33] R. Landauer, Conductance from transmission: Common sense points, *Phys. Scr.* **T42**, 110 (1992).
- [34] J. C. Duda, J. L. Smoyer, P. M. Norris, and P. E. Hopkins, Extension of the diffuse mismatch model for thermal boundary conductance between isotropic and anisotropic materials, *Appl. Phys. Lett.* **95**, 031912 (2009).
- [35] Q. Song and G. Chen, Evaluation of the diffuse mismatch model for phonon scattering at disordered interfaces, *Phys. Rev. B* **104**, 085310 (2021).
- [36] R. Cheaito, J. T. Gaskins, M. E. Caplan, B. F. Donovan, B. M. Foley, A. Giri, J. C. Duda, C. J. Szejewski, C. Constantin, H. J. Brown-Shaklee *et al.*, Thermal boundary conductance accumulation and interfacial phonon transmission: Measurements and theory, *Phys. Rev. B* **91**, 035432 (2015).
- [37] Y. Zhang, D. Ma, Y. Zang, X. Wang, and N. Yang, A modified theoretical model to accurately account for interfacial roughness in predicting the interfacial thermal conductance, *Front. Energy Res.* **6**, 48 (2018).
- [38] P. E. Hopkins, M. Baraket, E. V. Barnat, T. E. Beechem, S. P. Kearney, J. C. Duda, J. T. Robinson, and S. G. Walton, Manipulating thermal conductance at metal-graphene contacts via chemical functionalization, *Nano Lett.* **12**, 590 (2012).

- [39] J. C. Duda, T. E. Beechem, J. L. Smoyer, P. M. Norris, and P. E. Hopkins, Role of dispersion on phononic thermal boundary conductance, *J. Appl. Phys.* **108**, 073515 (2010).
- [40] N. Yang, T. Luo, K. Esfarjani, A. Henry, Z. Tian, J. Shiomi, Y. Chalopin, B. Li, and G. Chen, Thermal interface conductance between aluminum and silicon by molecular dynamics simulations, *J. Comput. Theor. Nanosci.* **12**, 168 (2015).
- [41] M. Shen, W. J. Evans, D. Cahill, and P. Keblinski, Bonding and pressure-tunable interfacial thermal conductance, *Phys. Rev. B* **84**, 195432 (2011).
- [42] S. Kullback and R. A. Leibler, On information and sufficiency, *Ann. Math. Stat.* **22**, 79 (1951).
- [43] Q. He, Y. Xu, H. Wang, Z. Li, and Y. Zhou, Role of elastic phonon couplings in dictating the thermal transport across atomically sharp SiC/Si interfaces, *Int. J. Therm. Sci.* **204**, 109182 (2024).
- [44] T. Feng and X. Ruan, Four-phonon scattering reduces intrinsic thermal conductivity of graphene and the contributions from flexural phonons, *Phys. Rev. B* **97**, 045202 (2018).
- [45] J. Zheng, D. Shi, Y. Yang, C. Lin, H. Huang, R. Guo, and B. Huang, Anharmonicity-induced phonon hardening and phonon transport enhancement in crystalline perovskite, *Phys. Rev. B* **105**, 224303 (2022).
- [46] L. Lindsay, D. A. Broido, and T. L. Reinecke, First-principles determination of ultrahigh thermal conductivity of boron arsenide: A competitor for diamond? *Phys. Rev. Lett.* **111**, 025901 (2013).
- [47] T. Feng, L. Lindsay, and X. Ruan, Four-phonon scattering significantly reduces intrinsic thermal conductivity of solids, *Phys. Rev. B* **96**, 161201(R) (2017).
- [48] D. A. Broido, M. Malorny, G. Birner, N. Mingo, and D. A. Stewart, Intrinsic lattice thermal conductivity of semiconductors from first principles, *Appl. Phys. Lett.* **91**, 231922 (2007).
- [49] F. Knoop, T. A. R. Purcell, M. Scheffler, and C. Carbogno, Anharmonicity measure for materials, *Phys. Rev. Mater.* **4**, 083809 (2020).
- [50] F. Knoop, T. A. R. Purcell, M. Scheffler, and C. Carbogno, Anharmonicity in thermal insulators: An analysis from first principles, *Phys. Rev. Lett.* **130**, 236301 (2023).
- [51] A. Giri, J. L. Braun, and P. E. Hopkins, Implications of interfacial bond strength on the spectral contributions to thermal boundary conductance across solid, liquid, and gas interfaces: A molecular dynamics study, *J. Phys. Chem. C* **120**, 24847 (2016).
- [52] T. Jiang, X. Zhang, S. Vishwanath, X. Mu, V. Kanzyuba, D. A. Sokolov, S. Ptasinska, D. B. Go, H. G. Xing, and T. Luo, Covalent bonding modulated graphene-metal interfacial thermal transport, *Nanoscale* **8**, 10993 (2016).
- [53] T. Zhang, A. R. Gans-Forrest, E. Lee, X. Zhang, C. Qu, Y. Pang, F. Sun, and T. Luo, Role of hydrogen bonds in thermal transport across hard/soft material interfaces, *ACS Appl. Mater. Interfaces* **8**, 33326 (2016).
- [54] Y. Xu and Y. Zhou, Collaborative mechanisms boost the nanoscale boiling heat transfer at functionalized gold surfaces, *Int. J. Heat Mass Transfer* **210**, 124179 (2023).
- [55] Y. Xu, F. Duan, Z. Li, and Y. Zhou, Surface functionalization enabling highly effective phase-change heat transfer of R1234yf: A molecular dynamics study, *Appl. Therm. Eng.* **240**, 122275 (2024).
- [56] M. D. Losego, M. E. Grady, N. R. Sottos, D. G. Cahill, and P. V. Braun, Effects of chemical bonding on heat transport across interfaces, *Nat. Mater.* **11**, 502 (2012).
- [57] R. Prasher, Acoustic mismatch model for thermal contact resistance of van der Waals contacts, *Appl. Phys. Lett.* **94**, 041905 (2009).
- [58] S. Sadasivam, U. V. Waghmare, and T. S. Fisher, Phonon-eigenspectrum-based formulation of the atomistic Green's function method, *Phys. Rev. B* **96**, 174302 (2017).
- [59] M. P. Allen and D. J. Tildesley, *Computer Simulation of Liquids*, 2nd ed. (Oxford University Press, Oxford, 2017).
- [60] S. Plimpton, Fast parallel algorithms for short-range molecular dynamics, *J. Comput. Phys.* **117**, 1 (1995).
- [61] C. Kittel, *Introduction to Solid State Physics*, 8th ed. (Wiley, Hoboken, 2005).